The Meteoritical Society

Meteoritics & Planetary Science 43, Nr 8, 1399–1414 (2008)
Abstract available online at http://meteoritics.org

Partial melting of H6 ordinary chondrite Kernouvé: Constraints on the effects of reducing conditions on oxidized compositions

Rena L. FORD[1, 2], Gretchen K. BENEDIX[3, 4*], Timothy J. McCOY[5], and Tracy RUSHMER[6]

[1]Department of Geological Sciences, University of Vermont, Burlington, Vermont 05405, USA
[2]Department of Earth and Planetary Sciences, University of New Mexico, Northrop Hall, Albuquerque, New Mexico 87131–1116, USA
[3]Department of Earth and Planetary Sciences, Washington University, Campus Box 1169, One Brookings Drive, Saint Louis, Missouri, 63130–4899, USA
[4]Department of Mineralogy, The Natural History Museum, Cromwell Road, London, SW7 5BD, UK
[5]Department of Mineral Sciences, National Museum of Natural History, Smithsonian Institution, Washington, D.C., 20560–0119, USA
[6]Department of Earth and Planetary Sciences, GEMOC, Macquarie University, 2109 NSW, Australia
*Corresponding author. E-mail: greb@nhm.ac.uk
(Supplementary material is available online at http://meteoritics.org/Online%20Supplements.htm)

(Received 18 May 2007; revision accepted 15 February 2008)

Abstract–Partial melting experiments at temperatures of 950–1300 °C were conducted on the H6 chondrite Kernouvé under reducing conditions using CO-CO_2 gas mixing and graphite-buffered sealed silica tubes to examine the effect of reducing conditions during melting of starting materials that are more oxidized relative to the oxygen fugacity conditions of the experiments. The experiments produced a range of mineralogical and compositional changes. Olivine exhibits significant reduction to compositions of $Fa_{2–5}$ at temperatures of 1300 °C. In contrast, orthopyroxene exhibits only slight reduction until the highest temperatures. Chromite is sometimes consumed by intruding sulfides, and displays increasingly magnesian compositions ranging as low as Fe/Fe + Mg of 0.1 at a constant Cr/Cr + Al ratio. The compositional changes with increasing temperature reflect a complex set of reactions, including oxidation-reduction. One application of these experiments address whether primitive achondrites could have formed from ordinary chondrite-like precursors by partial melting under reducing conditions. While changes observed in olivine and troilite compositions might support such an idea, differences in oxygen isotopic composition, Cr/Cr + Al in chromite, orthopyroxene compositions, and thermodynamic evidence against reduction during melting of primitive achondrites (Benedix et al. 2005) firmly refute such an idea.

INTRODUCTION

The range of meteoritic materials observed today is diverse in terms of both composition and geologic history. This diversity resulted from the interplay between the materials present in the early solar nebula and the processes that altered them to the solid bodies we observe today as asteroids. In some cases, the degree of alteration is such that any remnant of the precursor material was erased by subsequent geologic processes (e.g., partial melting, fractional crystallization, and aqueous alteration). But in cases where the degree of alteration is smaller, difficulty in determining the precursor may be due to overprinting of other processes. One way to address this is to conduct experiments on a variety of starting materials under different physical conditions. In this study, we examine the effect of partial melting of an oxidized (relatively speaking) chondritic precursor under reducing conditions (IW-3 and C-CO [1 bar]), in part testing a hypothesis for the formation of some primitive achondrites suggested by Kracher (1985).

EXPERIMENTAL METHODS

Chondritic Starting Material

We used the Kernouvé (H6; Fig. 1) ordinary chondrite for our experiments. As an H chondrite, Kernouvé contains abundant metal, allowing us to track metal migration during melting and, as a type 6 chondrite, it is chemically equilibrated to allow easy comparison between the starting and final mineral compositions. It is texturally metamorphosed and similar to what we would expect of any chondrite heated for a significant period of time before the onset of partial melting. Low shock type was also desired to

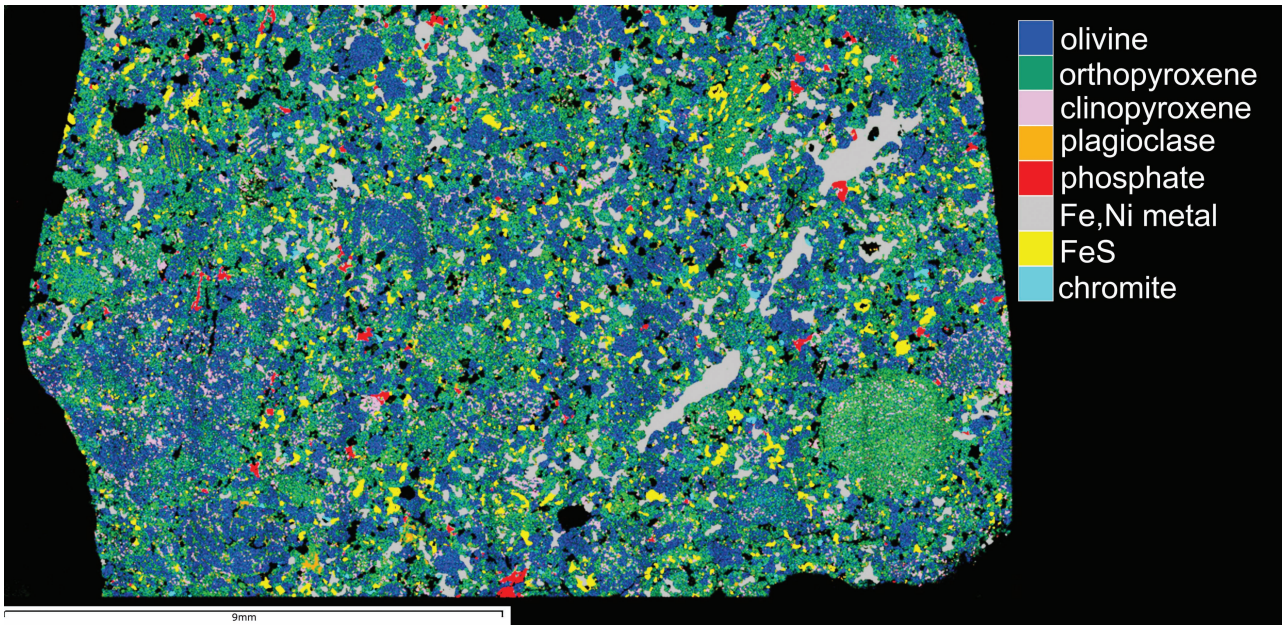

Fig. 1. Combined X-ray element map image showing starting texture and mineralogy of Kernouvé (PTS USNM 1054-2). Olivine is the dominant silicate, followed by orthopyroxene. This shows typical ordinary chondrite type 6 textures, with fading chondrule outlines and lack of matrix. Large, irregular composites of Fe,Ni metal, FeS, and chromite are observed. Phosphate is minor and distributed randomly throughout the section. Scale bar is 9 mm.

minimize complications from pre-experiment, shock-induced, metal-sulfide melt mobility. Kernouvé is minimally shocked (shock stage S1 using the scheme of Stöffler et al. 1991), although Rubin (2003) suggested that Kernouvé may have been more extensively shocked and subsequently annealed. Kernouvé has limited terrestrial weathering since it was an observed fall in 1869. Finally, it is well characterized both chemically and mineralogically (Hutchison 1981).

Experimental Techniques

Our experiments were designed to examine reduction during heating and partial melting of an oxidized (relative to primitive achondrites) chondrite. We defined our T-fO_2 ranges to replicate those experienced by partially melted, reduced primitive achondrites. Brett and Sato (1984) calculated intrinsic oxygen fugacities for chondrites and found that ordinary chondrites plot ~1 log unit below the iron-wüstite (Fe-FeO) buffer, while enstatite chondrites plot near the buffer curve for Cr-Cr_2O_3 (Fig. 2). Benedix et al. (2005) used 2-pyroxene temperatures to calculate the fO_2 conditions recorded by Winona and silicates in IAB irons near the peak temperatures experienced by these meteorites. These temperatures and fugacities are also shown in Fig. 2. The calculated fugacities at these temperatures are on a line that lies ~2.5 log units below the Fe-FeO buffer and therefore slightly above the buffer used in the gas mixing experiment (see below). A summary of the experimental conditions is listed in Table 1. Throughout the paper, when the term "oxidized" is used, we mean a composition that is oxidized relative to the oxygen fugacities of the experiments.

To understand the affect of a reducing environment on oxidized starting material, we conducted two sets of experiments. The first exploited the position of the 1 bar C-CO buffer as a control on oxygen fugacity and were conducted in sealed silica tubes with solid graphite crucibles. The C-CO buffer produces an fO_2 similar to that obtained for IAB-winonaites at ~950 °C, but becomes ~2–3 log units more reducing at 1300 °C (Fig. 2). These sealed silica tube experiments were undertaken to minimize volatile loss. The second set was conducted in open alumina crucibles and utilized gas mixing to precisely control the oxygen fugacity within the desired range (~IW-3). Although the experiments were constrained to the correct fO_2 as a function of temperature, they suffered from possible volatile loss. The positions of these experiments in T-fO_2 space are also shown in Fig. 2.

Both sets of experiments were conducted in vertical Deltech gas-mixing furnaces with muffle tubes at the Smithsonian Institution. Temperatures were measured using a type B ($Pt_{94}Rh_6$-$Pt_{70}Rh_{30}$) thermocouple calibrated against the melting point of gold (1064.5 °C). Temperatures are accurate to ±5 °C. For the sealed silica tube experiments, chips of Kernouvé ranging from 200 to 500 mg were placed inside a graphite crucible, which was subsequently sealed inside an evacuated high-purity silica tube. Sufficient adsorbed oxygen remains within the evacuated tube to allow the buffer reaction to reach equilibrium. The sealed silica tubes were mounted on alumina rods and placed into the furnace. The experiments were conducted at 950, 1000, 1100, 1200, and 1300 °C for 120 h and quenched in cold water.

For the gas mixing experiments, 200–500 mg Kernouvé chips were placed into an alumina crucible that was hung

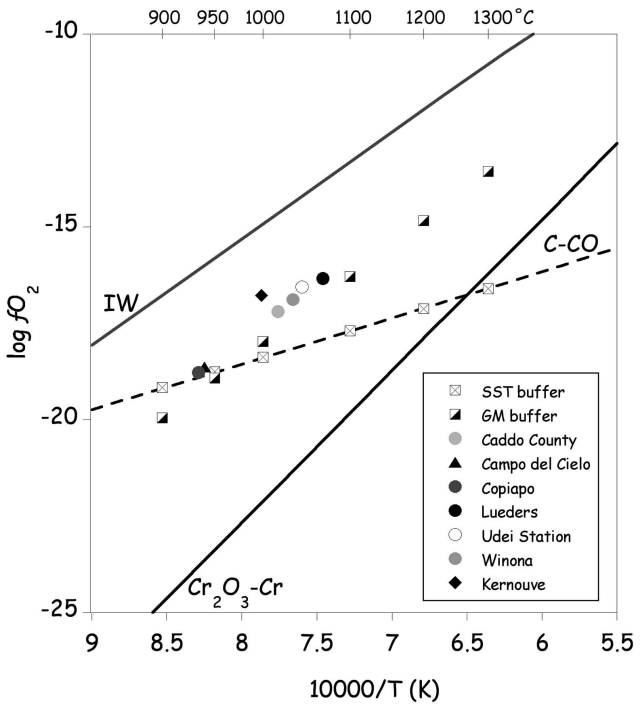

Fig. 2. Plot of log fO_2 versus 10,000/T (in K). Buffer curves for iron-wüstite (IW), Cr-Cr_2O_3, and C-CO (at 1 bar) are plotted. The IW and Cr-Cr_2O_3 buffers are used as proxies for the oxygen fugacity of ordinary and enstatite chondrites, respectively. Calculated values for Winona and several silicate-bearing IAB irons (from Benedix et al. 2005) define an oxygen fugacity of ~2.5 log units below IW at temperatures of ~900–1100 °C. The experiments were designed to bracket these conditions using sealed silica tube experiments (closed squares) along the C-CO buffer and open-system gas mixing (open squares) experiments at ~IW-3. Kernouvé intrinsic oxygen calculated using the method of Benedix et al. (2005) is also plotted for comparison.

from the bottom of the thermocouple, and flowing 1.2% CO_2 –98.8% CO gas was passed through the furnace. The oxygen fugacity of the system was calibrated using a yttria-stabilized zirconia ($(Y_2O_3)_{0.07}(ZrO_2)_{0.93}$) solid ceramic oxygen electrolyte cell. These experiments were run for 24 h at temperatures of 950, 1000, 1100, 1200, and 1300 °C and quenched with compressed air. We discuss the implications of the quench times below.

A single tank of pre-mixed gas (1.2% CO_2 in a balance-98.8% CO) was used for the experiments and with such a fixed composition gas, oxygen fugacity changes relatively little to standard buffers with temperature. This gas mixture yields oxygen fugacity conditions of 3.0 log units below the iron-wüstite buffer at 1100 °C, with deviation to IW-2.8 at 1300 °C and IW-3.2 at 950 °C (Table 1). Flowing gas was allowed to equilibrate within the furnace for 12 h prior to each run. Although the gas should yield an oxygen fugacity of IW-3.0, several sources of error may have been introduced into the system by our methods. In particular, it is important to note that the oxygen fugacity sensor is only rated for

Table 1. Summary of experimental conditions.

Experiment	Mass (mg)	T (°C)	Length (h)	log fO_2[1]	ΔIW
Gas mixing					
RF 10	172	950	24	−18.9	−3.1
RF 12	184	1000	24	−18.0	−3.1
RF 5	325	1100	24	−16.3	−3.0
RF 6	486	1200	24	−14.8	−2.9
RF 8	260	1300	24	−13.6	−2.8
Sealed silica tube					
RF 3	428	950	120	−18.8	−3.0
RF 1	269	1000	120	−18.4	−3.5
RF 7	170	1100	120	−17.7	−4.4
RF 2	380	1200	120	−17.1	−5.2
RF 11	112	1300	120	−16.6	−5.8

[1]log fO_2 is calculated using thermodynamic data.

temperatures up to 1600° and −16 log units fO_2, and the experimental study described here was conducted at the lower of the fO_2 range for the sensor cell. Gas mixing in the tank may have been less than ideal and precipitation of carbon above the hotspot of the furnace was observed at these reducing conditions and could have produced a more oxidizing gas. We measured the oxygen fugacity produced in the hotspot of the furnace by the mixed gas at 1100 °C and found a value of IW-2.7, slightly more oxidizing than the ideal fugacity of IW-3.0 (Table 1). Thus, we suggest that oxygen fugacities are accurate to within ±0.5 log units, which is slightly above the normal stated uncertainty of ±0.3 log units. Given the uncertainty on the oxygen fugacities calculated for winonaites (Benedix et al. 2005), the uncertainty in absolute oxygen fugacity of our experiments is acceptable.

In addition to controlling oxygen fugacity, we calculated the sulfur fugacity of the experiments based on phase equilibria for the following equilibrium reaction.

$$2Fe + S_2(g) = 2FeS \quad (1)$$

The equilibrium constant as a function of temperature is expressed as:

$$\mathrm{Log}K_1 = \mathrm{Log}\left(\frac{2a_{Fes}}{2a_{Fe} \times f_{s_2}}\right) = \frac{8163.47}{T} - 3.07 \quad (2)$$

800 – 1300°C.

In these equations, T is the temperature in Kelvin, a_{FeS} is the activity of FeS in sulfide, a_{Fe} is the activity of Fe in metal, and fS_2 is the sulfur fugacity. The values for a_{FeS} and a_{Fe} were determined using the microprobe analyses of the metal and troilite phases. Log K data for FeS were derived from JANAF (1998) tables. Our calculations show that Kernouvé and all of our experiments are 0.1 log units off the Fe-FeS buffer suggesting that this buffer is controlling fS_2 in our experimental system.

Analytical Methods

Polished thick or thin sections of each experimental charge for each temperature step were examined and analyzed. Besides these, a polished thin section of unheated Kernouvé (USNM 1054-2) was also studied. All sections were examined optically in reflected light and areas of interest were photographed. In addition, X-ray element maps (see maps in supplemental section) of each section were produced using the JEOL JSM-5900LV scanning electron microprobe at the Natural History Museum (NHM) in London. Mineral modes were determined from the X-ray maps using Adobe Photoshop. Major and minor element compositions of olivine, orthopyroxene, chromite, troilite, metal, and silicate melt were obtained using the JEOL Superprobe 733 electron microprobe at Washington University and the Cameca SX-50 at the NHM. All mineral analyses were conducted with a fully focused beam and a 20 nA beam current. The accelerating voltage was either 15 (Washington University) or 20 (NHM) kV. Well-known mineral standards were used and the data were corrected with manufacturer-supplied ZAF routines.

Evaluating Equilibrium and Volatilization

Because these experiments were conducted under reducing conditions and the effect of these conditions on olivine is quite pronounced (i.e., zoned olivine is produced), we used the composition of orthopyroxene to test for equilibrium. As discussed in more detail in the results section, the composition of orthopyroxene is invariable except in the case of the 1300° sealed silica tube experiment. In the cases where silicate melt was present (in the higher temperature runs), we also looked at Fe/Mg olivine/liquid exchange coefficient ($^{Ol/liq}K_{DFeO/MgO}$). In this case, the K_D for our gas mixing experiment (0.39) is similar to that of Jurewicz et al. (1995) (0.36 at 1300 °C). However, the sealed silica tube experiment Kd (0.24) differs significantly from equilibrium values. The lack of equilibrium in the sealed silica tube experiments is accompanied by significant loss of the volatile elements Na, K, and S, a topic we discuss in more detail in the results section of the paper. We recognize, however, that the formation of primitive achondrites may not have been an equilibrium process and, therefore, these experiments may offer additional insights. As discussed later, Feldstein et al. (2001) applied disequilibrium experiments to the formation of primitive achondrites.

RESULTS

Kernouvé is a typical H6 ordinary chondrite (Fig. 1), containing relict chondrules set in a coarse-grained, recrystallized matrix of olivine, orthopyroxene, plagioclase, Fe-Ni metal, troilite, chromite and phosphates. The distribution of these phases is typically heterogeneous at the thin or thick section scale. Mineral maps and detailed textural descriptions of all the experiments are provided in the online supplemental material at http://meteoritics.org/Online%20Supplements.htm.

The experiments produced both textural and compositional changes with increasing temperature. The results are presented in the context of five diagnostic minerals: olivine, low-Ca pyroxene, chromite, troilite and metal. We also briefly describe silicate melt that formed in the highest temperature experiments.

Textural Variations with Heating

Gross textural variations are illustrated in Fig. 3. In general, as temperature increases, we note that olivine shows very little change texturally, with the grains rounding only slightly relative to the original texture in Kernouvé (Figs. 3a–d). Orthopyroxene shows a range of textures from unaltered (Figs. 3a and 3b) to rounded grains or vein-like (Fig. 3c), although in the highest temperature fraction, the pyroxene takes on the form of rounded, zoned grains embedded in silicate melt (Fig. 3d). Metal texture does not change with temperature, however starting at 1000° in both sets of experiments, it clearly shows reaction where it is in contact with troilite. In extreme cases, there is reaction between metal, chromite, and troilite. At the highest temperatures, rounded (clearly melted and migrated) metal is found at the edges of the experiments. Chromite, especially in the sealed silica tube experiments, shows evidence of reaction even at the lowest temperature (Fig. 3a), with troilite veins cross-cutting chromite grains. With increasing heating, a chromite-troilite melt intergrowth texture is found (Fig. 3b). At 1100 °C (Fig. 3c), chromite shows evidence of zoning to a more Mg and Al-rich rim, but lacks the intergrowth texture seen at lower temperatures. At higher temperatures, chromite is highly zoned. Troilite shows evidence of melting and migration at the lowest temperature (Fig. 3a), reaction with chromite at moderate temperatures, and intergrowth with Fe,Ni metal at the highest temperatures (Figs. 3b–d). Void space is present in all temperature steps, although the voids themselves have a more rounded outline at higher temperatures.

Changes in Modal Abundances with Heating

Mineral modes for Kernouvé, the experimental charges, and average H-chondrite (from McSween et al. 1991) are listed in Table 2. Although thin sections may not be wholly representative of the entire rock, several interesting changes in mineralogy are noted with increasing temperature. Relative to average H-chondrite (McSween et al. 1991), our section of Kernouvé shows an enrichment of olivine and orthopyroxene, and a depletion of clinopyroxene, plagioclase, metal, and

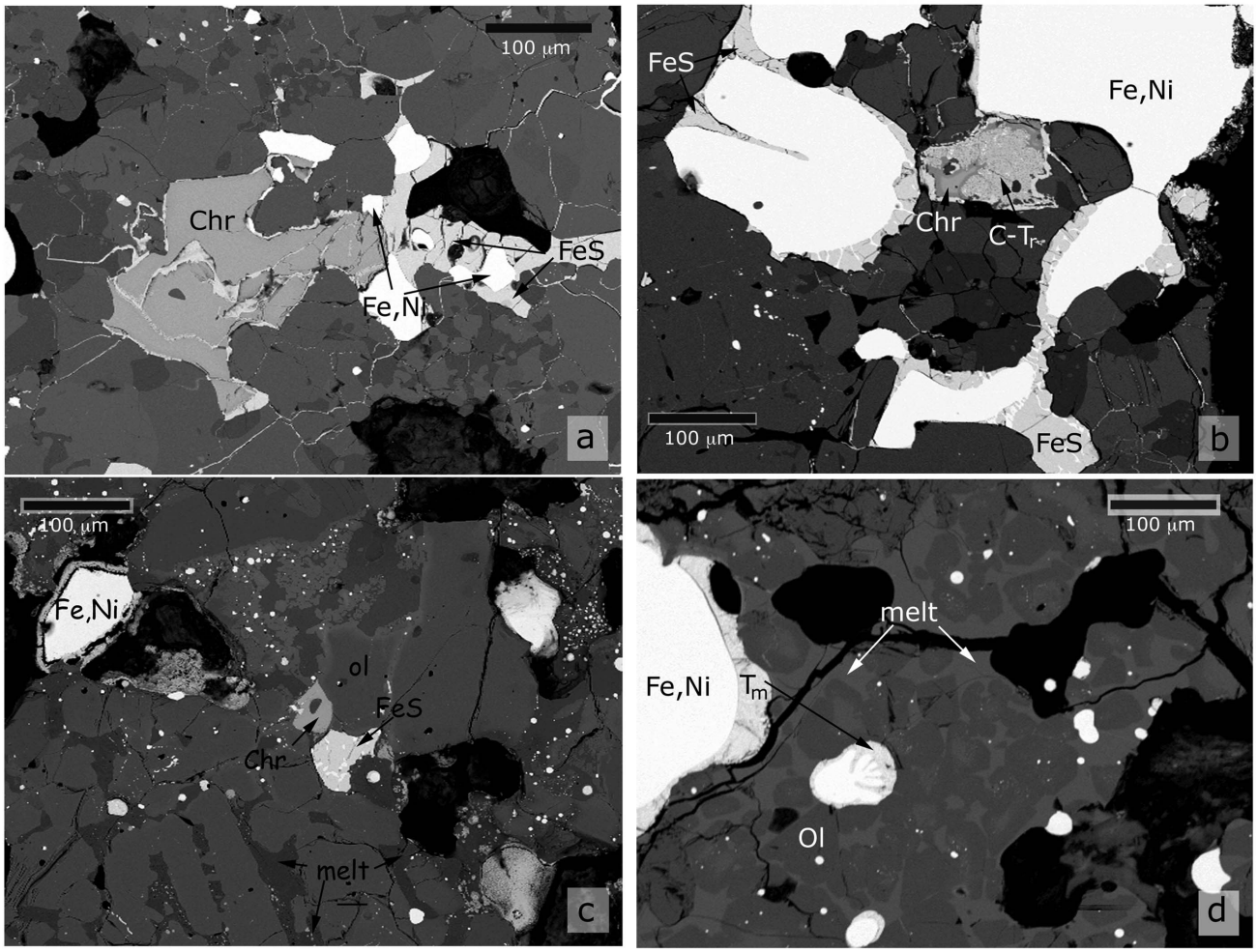

Fig. 3. Backscattered electron (BSE) images illustrating textures of the experiments. a) 950 °C (sealed silica tube). Fe,Ni-FeS melting has produced extensive areas of metal-sulfide intergrowth. Troilite migration is extensive and troilite veins penetrate, but have not reacted with, solid chromite (chr), olivine (ol), and plagioclase (pl). The black areas are holes; b) 1000 °C (sealed silica tube). Extensive Fe,Ni-FeS melting produced metal (Fe,Ni) blebs rimmed by troilite (FeS). Troilite rims and has reacted with chromite (chr), producing compositional zoning in chromite and a chromite-troilite reaction (C-Tr); c) 1100 °C (gas mixing). Melting of the opaque assemblage produced metal spheres rimmed by and intergrown with sulfide and reduction of chromite as a result of reaction with sulfide, while silicate melting (melt) produced FeO-rich crystallites on olivine rims; d) 1300 °C (sealed silica tube). Most of the silicate has melted (melt) with only a few vestigial olivine (ol) grains remaining. Troilite exists only in a troilite-Fe,Ni metal melt mixture (T_m).

troilite. The 950 °C and 1000 °C gas mixing experiment steps show modes that are within error of average H chondrite. Bearing this in mind, there are still some noteworthy variations. In the gas mixing experiments there is an overall increase in olivine and a decrease in clinopyroxene, plagioclase and metal abundances. There is a change in amount of chromite (decreasing from ~1 to 0.5%). Troilite also decreases in abundance by half. Orthopyroxene and phosphate show no consistent increase or decrease, but this is likely attributable to heterogeneous distribution of these minerals. Orthopyroxene abundance in the sealed silica tube experiments increases (Table 2) with a correlated decrease in olivine (Table 2) with temperature. There is an overall decrease in clinopyroxene (except at 1200°), chromite, metal, and troilite.

Chemical Changes with Heating

A summary of the marker mineral average compositions is listed in Table 3, while representative analyses of minerals from each experiment are listed in Tables 4 through 9. Compositional changes with temperature vary from slight to major for the different minerals.

Olivine

Data for olivine are listed in Table 4 and illustrated in Fig. 4a, which plots temperature versus Fa. In each experiment, cores and rims for several grains were analyzed in addition to randomly chosen grains. Overall, cores became slightly more ferroan relative to Kernouvé olivine, with increasing temperature. In the gas mixing experiments

Table 2. Mineral modes for Kernouvé and each experiment.

		Gas mixing					Sealed silica tube					
Mineral phase	Kernouvé	950°	1000°	1100°	1200°	1300°	950°	1000°	1100°	1200°	1300°	Avg. H chondrite[1]
Orthopyroxene	29.5	31.4	27.6	32.8	39.4	26.0	36.9	44.5	42.5	48.2	63.5	26.2
Olivine	46.8	37.1	37.6	42.1	35.7	46.9	43.8	32.3	37.7	28.3	18.8	35.0
Clinopyroxene	0.5	2.0	4.5	1.3	1.2	0.0	1.2	2.9	3.3	8.3	np	4.1
Plagioclase	4.8	10.6	10.3	5.7	4.1	1.6	2.0	9.8	5.8	4.2	np	9.6
Phosphate	0.9	0.8	0.7	3.5	np	np	0.5	np	np	np	np	0.7
Fe*	12.5	15.4	16.0	7.3	8.4	5.0	11.8	8.5	9.5	6.9	6.5	18.0
Troilite	4.0	1.9	2.5	2.5	0.8	2.4	3.2	1.8	1.0	1.8	2.4	5.5
Chromite	0.9	0.7	0.8	4.9	0.5	0.5	0.7	0.1	0.1	0.1	np	0.8
Silicate melt	np	np	np	np	9.9	17.7	np	np	np	2.3	8.8	
ol/opx	1.58	1.18	1.36	1.28	0.90	1.81	1.19	0.73	0.89	0.59	0.30	1.34

Fe* = Fe,Ni metal + weathering products.
np = Not present.
[1]From McSween et al. (1991).

(closed symbols in Fig. 4a), the cores of olivine have an average Fa value of ~18.5 mol% up to 1300 °C, where that value drops to ~Fa_{13}. Rims are slightly reduced relative to cores in the 950 °C and 1000 °C temperature steps, having an average Fa value of 17.3 mol%. Rims of olivine in the 1100 °C step are FeO-rich ($Fa_{23.3}$) compared to cores ($Fa_{19.4}$). On the whole, the gas mixing experiments reduced the olivine by an average of 6 mol% from lowest to highest temperature.

Reduction of olivine in the sealed silica tube (open symbols in Fig. 4a) experiments is more pronounced and occurs at a lower temperature. Average rim and core analyses indicate that the olivines are unzoned at the 1000 °C step, although the range of bulk olivine values spans 3.5 mol% ($Fa_{17.8}$ to $Fa_{21.2}$). The 1100 and 1200 °C experiments exhibit significant core to rim zoning, with magnesian rims and ferroan cores. Olivine in 1300 °C step has the lowest average Fa value at ~4 mol% of all the experiments, although we did not measure core and rim values.

Orthopyroxene

Cores, rims, and random grains of low-Ca pyroxene were measured in each experiment. Representative analyses are listed in Table 5. Figure 4b illustrates the variation, or more precisely the lack of variation, in FeO concentration (Fs) with temperature. Unlike olivine, average orthopyroxene compositions (cores, $Fs_{16.8}$; rims, $Fs_{17.0}$) do not change with increasing temperature in the experiments. The only sample that showed more magnesian compositions (average core = $Fs_{6.6\pm4.4}$; average rim = $Fs_{9.2\pm6.1}$) is the 1300 °C step in the sealed silica tube experiments.

Chromite

Table 6 lists the representative compositions of the chromite, while Fig. 5 illustrates bulk Cr/Cr + Al versus Fe/Fe + Mg for chromite grains in the experiments. Cr/Cr + Al shows only a slight decrease with increasing temperature. All charges except the 1300° step of the sealed silica tube experiments contained chromite. With increasing temperature, Fe/Fe + Mg decreases from ~0.85 to ~0.40 in the gas mixing experiment and from ~0.85 to ~0.10 in the sealed silica tube experiments. It is interesting to note that in the gas mixing experiments, except for one grain in the 1300° step, the chromites in the 1100° step are the most magnesian. Similar to olivine reduction begins at a lower temperature in the sealed silica tube experiments and proceeds quickly to lower Fe/Fe + Mg. These experiments show a sharp increase in MgO and decrease in FeO at the 1100° step, while in the gas mixing experiments, MgO and FeO decrease at such a rate as to keep the ratio nearly constant.

Troilite

Representative analyses of troilite are listed in Table 7. Many of the sulfide grains in the 1200° and 1300° steps were contained in a fine-grained, quenched texture of sulfide/metal melt (Fig. 3d). Sulfur concentrations are relatively invariant with increasing temperature, perhaps decreasing slightly at the higher temperatures and more prominently in the sealed silica tube experiments. Iron concentrations are more variable and generally 1–5 wt% below Kernouvé values. In contrast, Cr and Ni exhibit enrichments relative to Kernouvé at temperatures of 1000 °C and greater. Both Ni and Cr compositions in troilite are variable and likely controlled by the metal-melt textures. In detail, Ni shows a general increase with temperature, although the peak abundance is lower in gas mixing than in sealed silica. Chromium exhibits a more complicated pattern, initially increasing from the 950° to 1000° experiments. This increase is followed by decrease in Cr concentration at higher temperature steps. Unlike Ni, the peak abundance is in the gas mixing experiments.

Metal

Analyses of metal are listed in Table 8. With temperature, the metal shows a number of enrichments and depletions that

Table 3. Averages and standard deviations (s.d.) of olivine, orthopyroxene, chromite, and troilite compositions for Kernouvé and at each temperature step for both the gas mixing and sealed silica tube experiments.

		Kernouvé	Gas mixing experiments					Sealed silica experiments				
Temperature			950°	1000°	1100°	1200°	1300°	950°	1000°	1100°	1200°	1300°
Olivine	Fa (mol%)	17.68	18.38	17.64	21.71	17.00	12.34	18.19	19.27	15.88	3.80	3.81
	s.d.	*0.91*	*0.86*	*1.29*	*6.03*	*2.30*	*2.41*	*1.61*	*0.98*	*3.92*	*2.00*	*1.33*
	n	10	8	9	12	21	21	11	9	10	9	5
Orthopyroxene	Fa (mol%)	16.65	17.12	16.79	17.51	16.88	17.17	16.79	17.01	16.97	16.11	6.13
	s.d.	*0.30*	*0.23*	*0.25*	*0.34*	*0.35*	*0.15*	*0.15*	*0.52*	*0.28*	*0.99*	*4.80*
	n	11	10	8	7	10	2	10	10	7	9	44
Chromite	Fe/Fe + Mg (at%)	83.50	83.19	69.50	76.01	63.69	40.25	77.73	43.76	22.40	13.30	
	s.d.	*2.45*	*1.77*	*20.56*	*12.10*	*11.34*	*14.74*	*8.75*	*24.10*	*1.42*	*1.50*	
	Cr/Cr + Al (at%)	84.97	85.34	85.13	85.14	85.11	74.75	85.16	84.57	85.02	82.90	
	s.d.	*0.68*	*0.31*	*0.47*	*0.77*	*0.37*	*15.33*	*0.42*	*0.68*	*1.55*	*1.88*	
	n	19	9	12	12	11	13	11	10	9	11	
Troilite	Fe (wt%)	62.82	62.21	58.26	58.69	62.29	61.61	61.60	58.33	58.33	54.02	58.96
	s.d.	*0.46*	*0.65*	*1.82*	*2.59*	*3.35*	*0.83*	*0.46*	*1.93*	*0.97*	*9.05*	*3.35*
	S (wt%)	36.39	36.24	36.91	35.49	31.97	35.76	36.28	36.25	36.54	35.50	32.67
	s.d.	*0.26*	*0.15*	*0.49*	*1.88*	*5.47*	*1.89*	*0.35*	*0.26*	*0.39*	*2.17*	*3.75*
	Cr (wt%)	0.18	0.43	3.10	1.63	0.50	1.12	1.14	2.72	2.36	5.57	0.67
	s.d.	*0.37*	*0.66*	*1.65*	*1.36*	*0.68*	*0.81*	*0.82*	*1.83*	*0.66*	*7.42*	*0.45*
	Ni (wt%)	bdl	0.20	1.21	2.54	4.08	1.34	0.40	1.30	1.69	2.73	6.34
	s.d.		*0.09*	*0.36*	*1.86*	*4.17*	*0.79*	*0.07*	*0.58*	*0.46*	*5.21*	*4.41*
	n	24	16	15	13	23	16	19	23	19	14	15
Fe,Ni metal	Fe (wt%)	93.65	92.21	92.97	91.51	91.45	89.30	93.28	90.43	91.41	92.06	93.17
	s.d.	*0.87*	*1.19*	*0.46*	*1.55*	*1.27*	*3.19*	*0.71*	*0.51*	*0.91*	*0.60*	*1.56*
	Ni (wt%)	6.38	6.37	6.31	7.57	7.30	6.69	6.93	7.03	6.84	6.19	5.92
	s.d.	*0.26*	*0.25*	*0.38*	*1.81*	*1.04*	*3.19*	*0.52*	*0.27*	*0.69*	*0.45*	*1.14*
	P (wt%)	bdl	bdl	0.19	0.17	0.31	0.40	0.08	0.44	0.33	0.32	0.26
	s.d.			*0.05*	*0.15*	*0.11*	*0.28*	*0.04*	*0.02*	*0.21*	*0.09*	*0.13*
	Cr (wt%)	bdl	bdl	bdl	bdl	bdl	0.09	bdl	0.06	0.22	0.15	0.16
	s.d.						*0.03*		*0.04*	*0.15*	*0.07*	*0.03*
	n	26	10	10	10	10	10	9	13	9	15	22

bdl = Below detection limit.

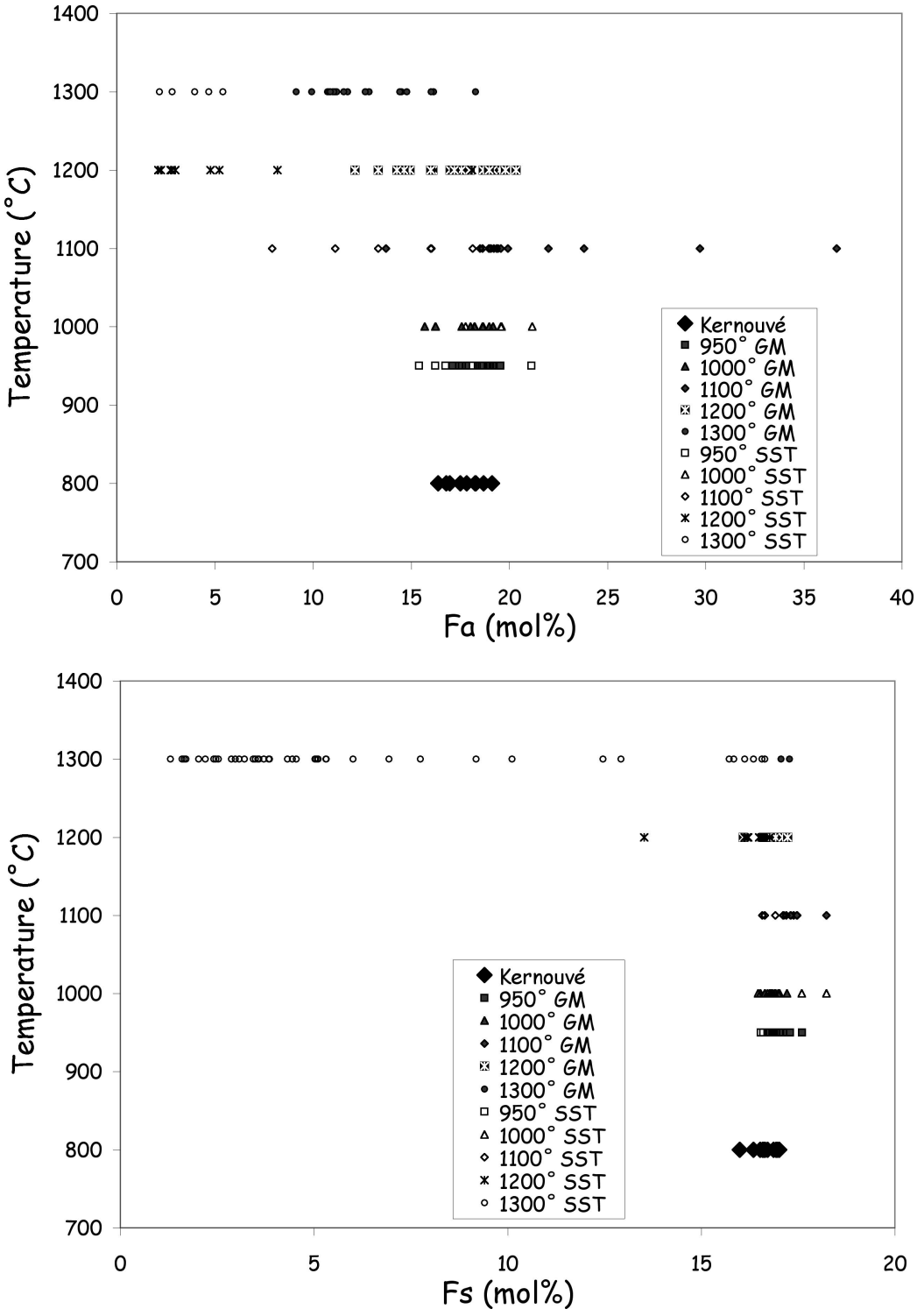

Fig. 4. a) Temperature versus olivine composition (Fa) for experiments and Kernouvé. Intrinsic Kernouvé fO_2 was determined using 800 °C as an approximation of peak metamorphic temperatures experienced by type 6 chondrites. Little compositional change is observed in heating to 1000 °C. At 1100 °C, most grains are unchanged, although some high-FeO olivines crystallized in the gas mixing experiment (see Fig. 3c) and reduction has begun in the sealed silica tube experiments. Reduction is apparent in both sets of experiments at 1200–1300 °C and more extensive in the sealed silica tube experiments. b) Temperature versus orthopyroxene composition (Fs) for experiments and Kernouvé. Compositions are essentially unchanged except for reduction in the 1300 °C sealed silica tube experiments.

Table 4. Representative analyses of olivine for Kernouvé and the gas mixing and sealed silica tube experiments. Core and rim compositions are shown for experiments where significant heterogeneity exists. Core and rim compositions are from single grains.

Temp.		Gas mixing								Sealed silica tube						
		950°	1000°	1100°		1200°		1300°		950°	1000°	1100°		1200°		1300°
	Kernouvé			Core	Rim	Core	Rim	Core	Rim			Core	Rim	Core	Rim	
SiO_2	38.69	38.48	39.32	38.90	37.97	39.70	40.28	38.75	40.01	39.43	38.96	38.72	39.72	39.80	40.43	42.01
Cr_2O_3	0.07	0.11	bdl	0.08	0.69	0.13	0.48	0.07	0.90	0.09	bdl	bdl	0.17	0.93	0.90	0.33
V_2O_3	bdl	bdl	bdl	bdl	bdl	bdl	bdl	0.05	bdl	bdl	bdl	0.05	bdl	bdl	0.06	0.08
FeO	16.99	17.07	17.52	18.27	20.10	17.38	11.50	17.23	12.17	16.98	18.17	18.13	12.75	4.78	3.01	2.85
MnO	0.44	0.50	0.45	0.50	0.53	0.46	0.50	0.48	0.61	0.43	0.53	0.40	0.46	0.56	0.65	0.42
MgO	43.93	42.46	42.93	42.12	39.99	42.44	46.70	43.24	47.03	42.95	41.92	42.39	46.57	53.44	54.85	54.96
CaO	bdl	bdl	bdl	bdl	0.06	bdl	0.31	0.05	0.15	bdl	bdl	bdl	bdl	0.13	0.25	0.14
ZnO	bdl	0.05	bdl	bdl	0.05	0.05	bdl	bdl	bdl	bdl	bdl	bdl	bdl	bdl	bdl	0.05
NiO	bdl	0.19	bdl	0.10	0.05	bdl	bdl	bdl	bdl	bdl	bdl	bdl	bdl	bdl	bdl	bdl
Total	100.13	98.85	100.22	99.97	99.43	100.17	99.78	99.93	100.96	99.93	99.58	99.69	99.67	99.67	100.22	100.83

bdl = Below detection limit.

Table 5. Representative analyses of orthopyroxene for Kernouvé and the gas mixing and sealed silica tube experiments.

Temp.		Gas mixing					Sealed silica tube				1300°	
		950°	1000°	1100°	1200°	1300°	950°	1000°	1100°	1200°		
	Kernouvé										Low Fe	High Fe
SiO_2	54.92	55.88	56.05	54.98	55.73	55.84	55.04	55.24	55.53	54.76	57.82	55.63
TiO_2	0.21	0.19	0.17	0.26	0.22	0.19	0.19	0.20	0.24	0.19	0.15	0.18
Cr_2O_3	0.42	0.12	0.48	0.81	0.29	0.20	0.47	0.03	0.55	0.61	0.64	0.16
Al_2O_3	0.17	0.14	0.14	0.32	0.13	0.17	0.18	0.11	0.15	0.19	0.58	0.16
FeO	11.29	11.55	11.04	12.04	10.87	11.28	11.22	12.35	11.48	11.30	2.45	11.18
MnO	0.52	0.45	0.45	0.52	0.45	0.52	0.51	0.40	0.49	0.47	0.41	0.51
MgO	31.14	30.62	30.74	29.29	31.17	29.63	30.69	30.70	30.65	31.53	36.55	30.86
CaO	0.79	0.76	0.75	1.39	0.88	0.93	0.94	0.49	0.70	0.80	0.96	0.99
Total	99.47	99.70	99.82	99.60	99.74	98.76	99.23	99.52	99.78	99.85	99.56	99.67

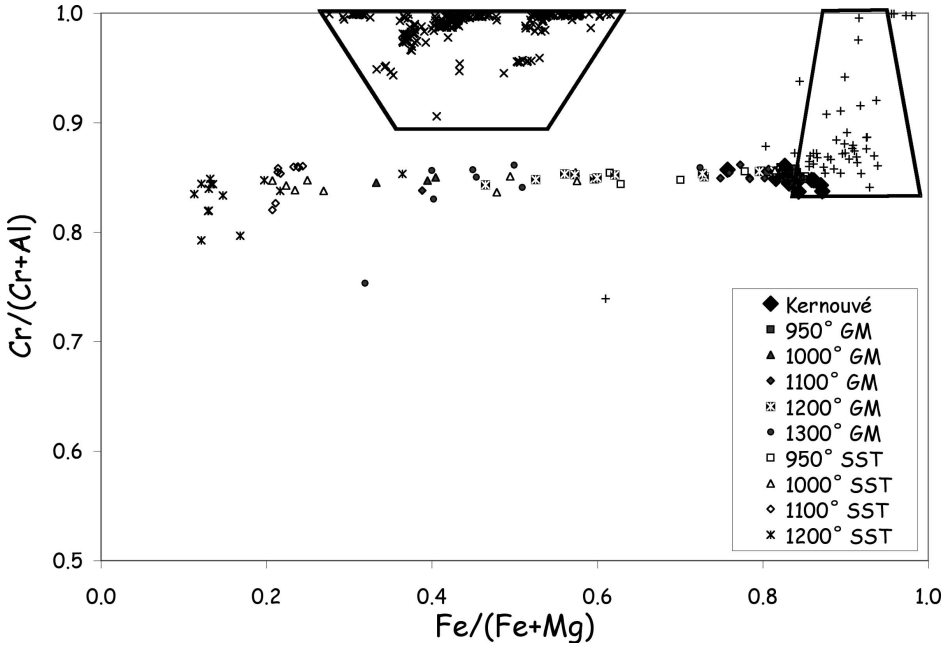

Fig. 5. Plot of Cr/Cr + Al versus Fe/Fe + Mg in chromites from ordinary chondrites (crosses) (data from Bunch et al. 1967), IAB irons/winonaites (x) (data from Benedix et al. 2005), Kernouvé and our experiments (this work). Ordinary chondrites exhibit a trend of decreasing Cr/Cr + Al at relatively constant Fe/Fe + Mg with increasing petrologic type. The type 6 chondrite Kernouvé plots at the lower end of this trend. In general, chromites in our experiment exhibit decreasing Fe/Fe + Mg at relatively constant Cr/Cr + Al with increasing temperature, although not in a monotonic fashion. The most magnesian compositions are observed in the sealed silica tube experiments. Note that the Kernouvé/experimental trend does not intersect the field for winonaites and IAB irons, which have higher Cr/Cr + Al values, suggesting that partial melting of a metamorphosed, ordinary chondrite precursor may not produce winonaites.

vary with experimental setup. In the gas mixing experiments, Fe decreases slightly with temperature, accompanied by a small increase in Ni. In the sealed silica tube experiments, Fe depletion is somewhat greater. In addition, almost all metal in the sealed silica tube experiments shows evidence of having reacted with troilite. In the metal-melt mixtures (Fig. 3d), the Fe content of metal is much lower (~75 wt%; 1200 °C Sealed Silica Tube experiment—Table 8) than in un-reacted metal and correlates with a higher Ni composition (~15–20 wt%). Co shows a similar pattern to Fe, in that there is a slight depletion in the gas mixing experiments with temperature, while the sealed silica tube experiments show a more complicated distribution. Phosphorus increases from below detection levels at the lower temperatures to nearly 1 wt% in the 1300° gas mixing experiment and is not correlated with Ni. Sulfur is only above detection limit (0.05 wt%) in a few grains of the metal-melt mixtures, and in those cases is correlated with increased Ni and decreased Fe (Table 8). Chromium is below detection limits in all gas mixing experiments except the highest temperatures, and then it only reaches 0.1 wt%. In contrast, chromium content of the metal starts increasing from the 1000 °C sealed silica tube experiments reaching a maximum of 0.5 wt% in the 1100 °C experiment. The higher temperature experiments have lower Cr contents. The reactions between metal, troilite, and chromite found in the sealed silica tube experiments account for the increased Cr compositions of the metal in these charges.

Silicate Melt

In addition to the variations seen in the four marker minerals, silicate melt was produced in the experiments. Melt is produced as early as the 1100° experiment in both sets of experiments. Given the lack of silicate melt at lower temperatures, we analyzed silicate melt in only the 1300 °C experiments where it was particularly abundant. Representative compositions are given in Table 9. The temperature at which silicate melt is produced and the compositions of the melt are consistent with basaltic partial melting. The melts have similar amounts of SiO_2, TiO_2, and Al_2O_3. There are significant differences in FeO, MgO, CaO, and Na_2O between the two experiments. FeO concentration of the silicate melts is lower in the 1300 °C sealed silica tube experiment relative to the 1300 °C gas mixing experiment. In contrast, MgO and CaO are higher in the sealed silica tube experiment than in the gas mixing experiment. The gas mixing experiment produced silicate melt with Na_2O of ~2.5 wt%, while the sealed silica tube experiment has sodium concentrations at the detection limit (~0.06 wt%).

DISCUSSION

In this section, we first explore the nature of the chemical and physical changes in the experiments; specifically, the controlling factors in the changes with temperature and the changes interlinked through common processes of oxidation-

Table 6. Representative analyses of chromite for Kernouvé and the gas mixing and sealed silica tube experiments.

Temp.		Gas mixing									Sealed silica tube					
		950°	1000°		1100°		1200°		1300°		950°		1000°		1100°	1200°
	Kernouvé		Core	Rim	Core	Rim	Core	Rim	Core	Rim	Core	Rim	Core	Rim		
TiO_2	1.97	2.02	2.10	2.30	2.07	1.99	2.14	2.07	2.22	2.35	2.04	2.16	2.00	2.21	2.72	2.06
Al_2O_3	6.20	6.39	6.34	7.04	6.55	6.56	6.39	6.68	6.40	6.73	6.47	6.63	6.49	7.47	7.08	8.01
Cr_2O_3	56.39	56.03	55.63	59.38	55.44	55.17	56.54	57.46	58.15	60.16	56.48	57.79	56.32	61.81	62.10	64.51
V_2O_3	0.94	0.84	0.79	0.86	0.82	0.85	0.80	0.87	0.89	0.92	0.85	0.85	0.84	0.98	0.96	0.78
FeO	29.18	28.89	28.49	14.73	29.34	27.84	28.45	22.44	25.77	16.77	28.71	22.65	28.54	9.59	8.20	5.03
MnO	0.84	0.92	0.91	1.21	0.69	0.80	0.75	0.60	0.69	0.60	0.83	0.49	0.92	0.84	0.73	0.90
MgO	3.41	3.05	3.29	12.17	3.10	4.30	3.64	7.69	5.51	11.53	3.35	7.96	3.31	16.19	16.95	18.43
ZnO	0.41	0.36	0.45	bdl	0.29	0.40	0.22	0.20	0.49	0.13	0.39	0.28	0.37	0.08	0.13	0.22
NiO	bdl	bdl	bdl	bdl	bdl	bdl	bdl	0.06	bdl	bdl	bdl	0.05	bdl	bdl	0.13	bdl
Total	99.34	98.51	98.01	97.70	98.30	97.92	98.92	98.06	100.11	99.19	99.11	98.86	98.80	99.17	98.99	99.93

bdl = below detection limit.

Table 7. Representative analyses of troilite for Kernouvé and the gas mixing and sealed silica tube experiments.

Temp.		Gas mixing					Sealed silica tube				
	Kernouvé	950°	1000°	1100°	1200°	1300°	950°	1000°	1100°	1200°	1300°
Fe	63.48	62.85	57.63	59.19	60.49	60.90	61.67	58.50	58.41	60.02	59.36
S	36.37	36.38	36.76	36.23	36.52	36.34	36.36	36.64	36.54	36.03	35.76
Cr	0.16	0.43	3.16	1.60	0.41	1.73	1.55	2.52	1.86	1.24	0.39
Mn	bdl	0.09	0.20	0.07	0.06	0.11	0.07	0.18	0.11	0.16	0.03
Ni	bdl	0.20	1.89	1.80	2.17	0.69	0.36	1.41	2.08	1.48	3.71
Total	100.01	99.96	99.63	98.89	99.65	99.77	100.01	99.25	99.01	98.93	99.25

bdl = below detection limit.

Table 8. Representative analyses of metal for Kernouvé and the gas mixing and sealed silica tube experiments.

Temp.		Gas mixing								Sealed silica tube								
		950°	1000°	1100°		1200°		1300°		950°	1000°		1100°		1200°		1300°	
	Kernouvé			Low-Ni	High-Ni	Low-Ni	High-Ni	Low-Ni	High-Ni		Low-Ni	High-Ni	Low-Ni	High-Ni	Low-Ni	High-Ni	Low-Ni	High-Ni
Fe	92.98	93.35	93.01	92.00	87.18	92.72	91.51	95.22	85.74	93.08	91.07	76.91	92.01	86.56	91.53	72.20	95.25	92.01
Co	0.47	0.46	0.45	0.47	0.77	0.48	0.54	0.04	0.39	0.48	0.45	0.50	0.41	0.40	0.32	0.23	0.34	0.40
Ni	6.42	6.34	6.63	7.45	12.41	6.57	9.48	0.82	10.11	6.55	6.85	20.29	6.94	13.32	6.90	26.58	3.56	7.24
P	bdl	bdl	0.20	0.11	0.08	0.19	0.47	0.29	0.31	0.14	0.44	0.68	0.26	0.35	0.43	0.65	0.36	0.71
Cr	bdl	bdl	bdl	bdl	0.04	bdl	bdl	0.12	0.09	bdl	0.05	0.07	0.54	0.28	0.10	bdl	0.15	0.09
S	bdl	bdl	bdl	bdl	bdl	bdl	bdl	bdl	bdl	bdl	bdl	0.25	0.02	0.16	0.06	0.11	bdl	0.06
Si	0.04	bdl	0.03	0.03	bdl	0.02	0.03	0.05	0.05	0.03	bdl	0.02	0.04	0.03	0.03	bdl	0.07	0.04
Total	99.91	100.15	100.32	100.05	100.49	99.97	102.02	96.54	96.69	100.28	98.86	98.72	100.22	101.10	99.37	99.77	99.72	100.55

§bdl = Below detection limit.

reduction or element mobility. In the latter part of this section, we briefly discuss in more detail how these changes can or cannot be interpreted in the context of the formation of reduced primitive achondrite meteorites.

A Synoptic View of Compositional-Textural Changes

In evaluating the changes in the experiments and the controls on these, we must address the fact that there were actually two sets of experiments, which differed in design and could, in theory, prove complementary. In practice, many of the changes observed are directly attributable to the differences in this experimental design. Most notable among these differences are the extent of reduction observed in olivine, chromite and, to a lesser extent, orthopyroxene. In each case, these phases in the sealed silica tube experiments were significantly more magnesian than in the comparable temperature step of the gas mixing experiments. Two possible causes exist for this difference. The first is the duration of these experiments. While the gas mixing experiments were run for 24 h, the sealed silica tube experiments were run for 120 h. In addition, the sealed silica tube experiments were conducted using solid graphite buffers to hold the experiments at the C-CO buffer. At temperatures of 1100 °C and above, the C-CO buffer becomes significantly (up to 3 log units) more reducing than the gas mixing experiments. Insufficient data exists to establish whether the observed differences in phase compositions result from differences in run time or fO_2. Sealed silica tube experiments conducted for 24 h might resolve this issue, but it seems likely that the compositional differences reflect both of these variations in run conditions.

The other major difference between the gas mixing and sealed silica tube experiments was the attempt to limit volatilization in the latter experiments. While both experiments would experience some volatilization, it was presumed that the sealed silica tube experiments would reach equilibrium between the experiment and the enclosing gas within the tube. The gas mixing experiments were open systems with flowing gas and continuous, extensive volatilization might occur, despite the limited run times. In both experiments, we were able to achieve our major objective of preventing complete volatilization of sulfur and loss of troilite. It appears that volatilization likely played a role in both sets of these experiments and, despite efforts to control it, it appears more prevalent in the sealed silica tube experiments. Within these experiments, we observe a slight decrease in the S concentration of the sulfide phase at 1200–1300 °C, as well as a depletion of troilite relative to H-chondrite and the gas mixing experiments (Table 7). Further, greater volatilization in the sealed silica tube experiments is also suggested by the composition of the silicate melt in the two experiments at 1300 °C. While the gas mixing experiment silicate melt contain ~2.5 wt% Na_2O, the sealed silica tube silicate melt at the same temperature is essentially devoid of Na_2O. Most noteworthy, however, is the decreasing olivine to orthopyroxene ratio (Table 2) with temperature, which suggests that Kernouvé reacted extensively with the silica tube during these experiments. Orthopyroxene forms at the expense of olivine in the presence of silica via the following reaction:

$$(Mg,Fe)_2SiO_4 + SiO_{2(gas)} = 2(Fe,Mg)SiO_3 \quad (3)$$

Enhanced volatilization in the sealed silica tube experiments likely reflects the longer run times, the lower oxygen fugacity, and reaction between the silica tube and graphite crucible to produce SiO_2 gas that reacted with the experimental charges (Tissandier et al. 2002). It is clear that the tube volatilized and subsequently reacted with the melting olivine to create orthopyroxene. Despite this overprinting of volatilization, changes in the sealed silica tube experiments are dominated by the effect of reduction during heating.

While the two sets of experiments may have differed in detail, they share some common features. The most noteworthy of these is changing iron abundance among phases. In general, the compositions of three of our important marker phases—olivine, orthopyroxene and chromite—exhibit more magnesian, less ferroan compositions with increasing temperature. These changes are most apparent in olivine and chromite and, owing to much lower diffusion rates, less pronounced in orthopyroxene. It seems apparent, particularly at the higher temperature that FeO is migrating from these minerals. The obvious driver for this is reduction as a result of our imposing low fO_2 conditions on the system. The presence of low-Ni metal within the high-temperature experiments (Table 8) suggests reduction of FeO to Fe^0, with associated liberation of oxygen.

Oxidation-reduction and elemental exchange also seem to occur as a result of the chromite-troilite reaction observed at temperatures of 1000–1300 °C. Elemental exchange is most easily detected in the increase in Cr concentration within the sulfide relative to Kernouvé (Table 7) at these temperatures. Although there is some Cr in metal in the starting compositions, it is generally below detection level of the electron microprobe and therefore the most ready source of chromium is chromite. Thus it would be easy to attribute the increase in Cr in troilite to diffusion of Cr_2O_3 from chromite as a result of the reducing conditions, reduction of chromium oxide to chromium and incorporation of that chromium into troilite. However, this explanation appears inconsistent with chromite compositions. Chromite compositions in these experiments exhibit only very slight deviations from the chondritic starting composition in Cr/Cr + Al. This undoubtedly results from the very slow diffusion rates of the trivalent cations within the chromite structure, particularly relative to the divalent cations Fe and Mg. Thus, chromite does not appear to be losing chromium. A more likely explanation is that chromite is simply being consumed by the intruding troilite. This consumption and reduction

Table 9. Representative analyses of silicate melt for the gas mixing and sealed silica tube experiments.

	Gas mixing	Sealed silica tube
Temp.	1300°	1300°
SiO_2	57.08	55.65
TiO_2	0.36	0.53
Al_2O_3	12.80	13.86
Cr_2O_3	1.36	0.77
FeO	6.95	3.46
MnO	0.51	0.60
MgO	10.56	11.94
CaO	5.97	12.58
NiO	0.07	0.11
Na_2O	2.33	0.06
K_2O	0.29	0.02
S	0.06	0.10
Total	98.34	99.68

could explain the increase in chromium within the troilite and is consistent with textural evidence from the troilite-chromite intergrowths.

There also exists evidence for limited oxidation in one of our marker minerals. At 950 and 1000 °C in both the gas mixing and sealed silica tube experiments, there are some olivines and low-Ca pyroxenes that exhibit compositions more FeO-rich than those observed in Kernouvé. The existence of these FeO-rich minerals is particularly apparent in the olivines of the 1100 °C gas mixing experiments. In this case, these FeO-rich olivines appear to have crystallized from the melt. In addition, these temperature steps lacked the Ni-poor metal observed at 1300 °C. The source of the Fe that produced these mafic silicates is unclear, but oxidation of metal by small amounts of adsorbed oxygen is one possible source. As temperature increased, adsorbed oxygen decreased, reducing conditions dominated, and these FeO-rich mafic silicates disappeared from the system.

Thus, we can explain the changes in our system—albeit imperfectly—as a result of oxidation-reduction and elemental exchange, often in response to the reducing conditions imposed upon the system and consistent with relative diffusion rates and phase equilibria within the system. The significant overall reduction observed with increasing temperature was balanced by oxidation of either the graphite crucible used in the sealed silica tube experiments or the CO gas that dominated the gas mixture used to control fO_2 in the gas mixing experiments.

Comparison to Other Partial Melting Experiments

A number of authors have conducted partial melting experiments on chondritic material and it is informative to compare our results to this body of previous work. The most common type of experiment attempts to reproduce equilibrium melting over a limited range of temperature and oxygen fugacity, primarily to understand melt genesis from a chondritic source. Jurewicz et al. (1991, 1995) reported such experiments with melting of the Allende CV3 carbonaceous chondrite and the St. Severin (LL) and Lost City (H) ordinary chondrites. Allende differs markedly in composition from the Kernouvé material we utilized, but Jurewicz et al. (1991) tried the innovative approach of varying fO_2 over 4 log units to examine the influence of oxygen fugacity on melt composition. While similar to our approach, these authors worked at more oxidizing conditions (IW-1 to IW + 2). Coupled with the FeO-rich nature of their starting composition, direct comparison of our experimental results is unwarranted. A more direct comparison can be made to the ordinary chondrite melting experiments of Jurewicz et al. (1995), conducted at 1150–1350 °C and fO_2 of IW-1. These authors did not observe significant changes in Fe/Mg ratio of residual olivine or pyroxene with increasing temperature. Additionally, these authors observed higher degrees of partial melting and melt compositions significantly poorer in SiO_2 and Al_2O_3 and substantially enriched in FeO compared to our experiments, most consistent with the more oxidized conditions of the Jurewicz et al. (1995).

The work of Feldstein et al. (2001) may be most directly applicable to our work in terms of motivation. These authors were interested in the processes operating during disequilibrium at low degrees of partial melting with application to the formation of the acapulcoite/lodranite primitive achondrites. Experimentally, these authors melted chips of the Leedey (L6) ordinary chondrite at a constant temperature (1200 °C) and fO_2 of IW-1 over a range of run durations from 1 h to 21 days. These authors did not observe systematic changes in Fe/Mg ratio of olivine and orthopyroxene with increasing run duration. Interestingly, their melt compositions in the 1 and 10 h experiments are broadly comparable to our 1300 °C gas mixing experiment silicate melt for SiO_2, Al_2O_3, and CaO, although our experiment has, as expected, higher MgO and lower FeO. With increasing run time (3–21 days), Feldstein et al. (2001) found silicate melts with lower SiO_2 and higher Al_2O_3 and CaO. While it is difficult to directly compare our results, this finding suggests that longer run times in our experiments might have produced melt compositions more comparable to those of Jurewicz et al. (1995), although we chose shorter run times to minimize sulfur volatilization.

To the best of our knowledge, no experiments on the melting of ordinary chondrites between ~IW-2 and ~IW−5 have been conducted. McCoy et al. (1999) conducted experiments on the melting of the Indarch (EH4) enstatite chondrite utilizing vanadium and chromium buffers. These buffers should maintain an fO_2 of ~IW-5 at the complete range of temperatures investigated by these authors (1000–1500 °C). It is interesting to compare our sealed silica tube experiments at 1200–1300 °C, which achieved fO_2 of IW-5.2 to IW-5.8, to those of McCoy et al. (1999). The experiments are similar in one regard, namely the amount of melt produced. However, the contrast is sharp and instructive. While our experiments that used Kernouvé may have

Table 10. Diagnostic attributes of silicate-bearing IAB irons/winonaites compared to H chondrites.

Attribute		Win/IAB	H chondrite
Olivine	Fa (mol%)	1.0–8.0	16.9–20.4
Orthopyroxene	Fs (mol%)	1.0–8.0	15.7–18.1
Chromite	Cr/(Cr + Al)	0.9–1.0	0.85
Chromite	Fe/(Fe + Mg)	0.4–0.6	0.85
Troilite	Cr (wt%)	~0.4	bdl[2]
Graphite abundance	wt%	~0.5–25	~0.07
Chondrules		Rare relic	Present
Peak T[1]		~950–1200 °C	~850–900 °C
Element behavior	Chromium	Lithophile and chalcophile	Lithophile
Element behavior	Phosphorous	Lithophile and siderophile	Lithophile

[1]Peak temperatures for Win/IAB from Benedix et al. (1998, 2000, 2005); Peak temperatures for H chondrites from Dodd (1980). [2]Below detection limit.

achieved comparable fO_2, they contain significant FeO in residual olivine and pyroxene and in the silicate melt, they lack silicon in the metal, and, although they incorporate significant quantities of chromium in sulfides, they lack Mg, Mn and Ca typically found in experiments that began with an enstatite chondrite starting material. These differences provide a cautionary note that short-duration experiments, while achieving local equilibrium, cannot fully reproduce the partial melting of an asteroid that occurred over much longer time scales or began with material intrinsically more oxidized or reduced than the experimental starting material. Thus, we approach the application of our experiments to the genesis of primitive achondrites (specifically Winonaites and the associated IAB iron meteorite group) with appropriate care.

Implications for Primitive Achondrites

The properties of primitive achondrites (Table 10) have long been taken to indicate formation at oxygen fugacities intermediate between ordinary chondrites and enstatite chondrites (e.g., Mittlefehldt et al. 1998). In addition to the FeO-poor mineral compositions, evidence for the reduced nature of these meteorites is provided by presence of minerals only formed at oxygen fugacities below that of ordinary chondrites. It is unclear how this reduced nature was established. Benedix et al. (2005) calculated T-fO_2 histories for pyroxene-pyroxene and olivine-chromite pairs in Winona and IAB silicate inclusions, observing that fO_2 (relative to IW) is similar over a range of temperatures. This suggests that only slight reduction occurred during metamorphism and implies a chondritic precursor initially more reduced than ordinary chondrites. In contrast, Kracher (1985) postulated that these meteorites might have been reduced from an oxidized starting composition during metamorphism, perhaps during heating to peak temperatures prior to metamorphism. We can use the results of our experiments to explore these contrasting hypotheses. We recognize that the oxygen isotopic composition of our ordinary chondrite starting material (Clayton et al. 1991) does not match that of the primitive achondrites (Clayton and Mayeda 1983, 1996), but that does not invalidate the idea that an oxidized chondritic precursor, such as a carbonaceous chondrite, could be reduced during melting, producing meteorites akin to primitive achondrites.

A key requirement of the Kracher hypothesis is the reduction of FeO from mafic silicates to produce magnesian compositions seen in primitive achondrites. We observe substantial changes in olivine composition with increasing temperature; becoming more magnesian and reaching values that overlap those of primitive achondrites at the 1300 °C temperature step. We calculate that similar changes could have occurred during partial melting at temperatures that were more typically 1000–1100 °C (Benedix et al. 1998, 2000, 2005), if we consider that slower diffusion rates (Misener 1974) are compensated by time scales on the order of tens of millions of years (Bogard et al. 1967; Niemeyer 1979; Wadhwa and Russell 2000). We speculate that reduction of orthopyroxene could also occur given these temperatures and time, although only modest changes were observed in our experiments. A significant limitation to oxidation is the source of reductant. In our experiments, the dominant reduction reaction is that of olivine reacting with graphite to form carbon monoxide, iron metal, and magnesian olivine. Given the abundance of olivine and its initial and final compositions within the sealed silica tube experiments, we calculate that ~0.5 wt% graphite is required. Natural systems are graphite-limited and ordinary chondrites typically contain <0.1 wt% C (Moore and Lewis 1965). This argues strongly that an oxidized chondritic precursor would have to be richer in carbon than that normally found in ordinary chondrites. Carbonaceous chondritic precursors would satisfy both the need for abundant graphite as well as similar oxygen isotopic signatures (Clayton and Mayeda 1983; Clayton et al. 1991).

Metal-sulfide melting is prominent in both the primitive achondrites and the experiments, providing a constraint on the nature of the precursor material. In our experiments, Fe,Ni-FeS melts reacted with chromite to incorporate chromium into the sulfide melt. The reduction of FeO from the mafic silicates did not result in a marked increase of Fe^0 in the metal, as indicated by the nearly constant average Ni concentrations (Table 3). Thus, partial melting during

reduction might provide a mechanism for the formation of the chromium sulfide daubreélite.

For the formation of primitive achondrites, the main feature that is inconsistent with the partial melting of an oxidized precursor under reducing conditions is chromite composition, specifically the trivalent cation ratio. In ordinary chondrites, chromite Cr/Cr + Al ranges from 1.0 in type 3 chondrites to 0.85 in type 6 chondrites like Kernouvé (Bunch et al. 1967). Chromite compositions in winonaites and IAB irons have Cr/Cr + Al that ranges from 0.95 to 1.0, while Fe/Fe + Mg ranges from 0.3 to 0.6 (Bunch et al. 1970; Benedix et al. 2005). In our experiments, chromite Cr/Cr + Al varies only marginally (Table 3), suggesting that trivalent cations are not redistributed during partial melting of a metamorphosed chondritic precursor. Thus, chromite Cr/Cr + Al appears to be inherited from the precursor and can be used as a diagnostic signature when trying to identify a likely chondritic parent.

CONCLUSIONS

Based on the experimental results derived here, reduction of FeO from silicates and incorporation of Cr into sulfides is possible given the right T-fO_2 history and presence of sufficient reductant. Thus, partial melting of an oxidized precursor under reducing conditions satisfies some aspects of primitive achondrite formation. However, the reacting phases (e.g., olivine, pyroxene, chromite) respond at markedly different rates and it is unclear whether a single T-fO_2 history can produce changes of the correct magnitude simultaneously. In addition, features such as the chromite composition cannot be explained by reduction alone. While modest reduction during metamorphism may have occurred during primitive achondrite formation, we conclude that the precursor chondrite was unlikely to have been as FeO-rich and oxidized as ordinary chondrites. Instead, the most likely precursor would have been only modestly more oxidized than current primitive achondrites, exhibited similar oxygen isotopic composition, have contained abundant metal and sulfide, and had chromite with similar Cr/Cr + Al. Such a chondrite is currently unknown. Although CR chondrites have a number of promising similarities (e.g., oxygen isotopic composition, oxidation state) and have been discussed as a parental material (Rubin 2006), the paucity of sulfide and chromite prohibits such a link. Partial melting of a carbonaceous chondrite prior to aqueous alteration might provide a suitable alternative.

Acknowledgments–Samples of Kernouvé were kindly provided by the Smithsonian Institution. Expert technical assistance was provided by T. Gooding. Helpful advice and discussions about the experimental technique were provided by Gary Lofgren. Constructive discussions with Cari Corrigan and Dante Lauretta and comments on an early version by K. Righter, A. Kracher, and an anonymous reviewer improved the manuscript. Reviews by H. Connolly and J. Boesenburg are greatly appreciated. This study was funded in part by NASA grants NAG5-10463 (TR) and NAG5-13464 (TJM); the Vermont Space Grant Consortium and the Becker Endowment to the Smithsonian Institution.

Editorial Handling—Dr. Kevin Righter

REFERENCES

Benedix G. K., McCoy T. J., Keil K., Bogard D. D., and Garrison D. H. 1998. A petrologic and isotopic study of winonaites: Evidence for early partial melting, brecciation, and metamorphism. *Geochimica et Cosmochimica Acta* 62:2535–2553.

Benedix G. K., McCoy T. J., Keil K., and Love S. G. 2000. A petrologic study of the IAB iron meteorites: Constraints on the formation of the IAB-Winonaite parent body. *Meteoritics & Planetary Science* 35:1127–1141.

Benedix G. K., Lauretta D. S., and McCoy T. J. 2005. Thermodynamic constraints on the formation conditions of Winonaites and silicate-bearing IAB irons. *Geochimica et Cosmochimica Acta* 69:5123–5131.

Bogard D. D., Burnett D., Eberhardt P., and Wasserburg G. J. 1967. ^{40}Ar-^{40}K ages of silicate inclusions in iron meteorites. *Earth and Planetary Science Letters* 3:275–283.

Brett R. and Sato M. 1984. Intrinsic oxygen fugacity measurements of 7 chondrites, a pallasite, and a tektite and the redox state of meteorite parent bodies. *Geochimica et Cosmochimica Acta* 48: 111–120.

Bunch T. E., Keil K., and Snetsinger K. G. 1967. Chromite composition in relation to chemistry and texture of ordinary chondrites. *Geochimica et Cosmochimica Acta* 31:1569–1582.

Bunch T. E., Keil K., and Olsen E. J. 1970. Mineralogy and petrology of silicate inclusions in iron meteorites. *Contributions to Mineralogy and Petrology* 25:297–340.

Clayton R. N. and Mayeda T. K. 1983. Oxygen isotope relationships in iron meteorites. *Earth & Planetary Science Letters* 65:229–232.

Clayton R. N., Mayeda T. K., Goswami J. N., and Olsen E. J. 1991. Oxygen isotope studies of ordinary chondrites. *Geochimica et Cosmochimica Acta* 55:2317–2337.

Clayton R. N. and Mayeda T. K. 1996. Oxygen isotope studies of achondrites. *Geochimica et Cosmochimica Acta* 60:1999–2018.

Dodd R. T. 1980. *Meteorites: A chemical-petrologic synthesis.* Cambridge: Cambridge University Press. 368 p.

Feldstein S. N., Jones R. H., and Papike J. J. 2001 Disequilibrium partial melting experiments on the Leedey L6 chondrite: Textural controls on melting processes. *Meteoritics & Planetary Science* 36:1421–1441.

Hutchison R., Bevan A. W. R., Easton A. J., and Agrell S. O. 1981. Mineral chemistry and genetic relations among H-group chondrites. *Proceedings of the Royal Society of London Series A* 374:159–178.

JANAF 1998. *Thermochemical tables*, 4th ed. *Journal of Physical and Chemical Reference Data*. Monograph 9.

Jurewicz A. J. G., Mittlefehldt D. W., and Jones J. H. 1991. Partial melting of the Allende (CV3) meteorite—Implications for origins of basaltic meteorites. *Science* 252:695–698.

Jurewicz A. J. G., Mittlefehldt D. W., and Jones J. H. 1995. Experimental partial melting of the St. Severin (LL) and Lost City (H) chondrites. *Geochimica et Cosmochimica Acta* 59:391–408.

Kracher A. 1985. The evolution of the partially differentiated planetesimals: Evidence from the iron meteorite groups IAB and IIICD. *Journal of Geophysical Research* 90:C689–C698.

McCoy T. J., Dickinson T. L., and Lofgren G. E. 1999. Partial melting

of the Indarch (E4) meteorite: A textural, chemical, and phase relations view of melting and melt migration. *Meteoritics & Planetary Science* 34:735–746.

McSween H. Y., Bennett M. E., and Jarosewich E. 1991. The mineralogy of ordinary chondrites and implications for asteroid spectrophotometry. *Icarus* 90:107–116.

Mittlefehldt D. W., McCoy T. J, Goodrich C. A., and Kracher A. 1998. Non-chondritic meteorites from asteroidal bodies. In *Planetary materials*, edited by Papike J. J. Washington, D.C.: Mineralogical Society of America. pp. 4-1–4-193.

Misener D. J. 1974. Cationic diffusion in olivine to 1400 °C and 35 kbar. *Geochemical transport and kinetics*, edited by Hoffmann A. W. Washington, D.C.: Carnegie Institute. pp. 117–129.

Moore C. B. and Lewis C. F. 1965. Carbon abundances in chondritic meteorites. *Science* 149:317–318.

Neimeyer S. 1979. ^{40}Ar-^{39}Ar dating of inclusions from IAB iron meteorites. *Geochimica et Cosmochimica Acta* 43:1829–1840.

Rubin A. E. 2003. Chromite-plagioclase assemblages as a new shock indicator; implications for the shock and thermal history of ordinary chondrites. *Geochimica et Cosmochimica Acta* 67: 2695–2709.

Rubin A. E. 2006. Shock features in acapulcoites and lodranites: Implications for the origin of primitive achondrites (abstract #1090). 37th Lunar and Planetary Science Conference. CD-ROM.

Stöffler D., Keil K., and Scott E. R. D. 1991. Shock metamorphism of ordinary chondrites. *Geochimica et Cosmochimica Acta* 55: 3845–3867.

Tissandier L., Libourel G., and Robert F. 2002. Gas-melt interactions and their bearing on chondrule-formation. *Meteoritics & Planetary Science* 37:1377–1389.

Wadhwa M. and Russell S. S. 2000. Time scales of accretion and differentiation in the early solar system: The meteoritic evidence. In *Protostars and planets IV.* Edited by Mannings V., Boss A. P., and Russell S. S. Tucson: The University of Arizona Press. pp. 995–1018.